JOURNAL OF APPLIED CRYSTALLOGRAPHY
ISSN 1600-5767

System for *in situ* observation of three-dimensional structural changes in polymer films during uniaxial deformation

Tsukasa Miyazaki,[a]* Keisuke Shimokita,[a] Hiroki Ogawa[b] and Katsuhiro Yamamoto[c]

[a]Functional Design Technology Center, Nitto Denko Corporation, 1-1-2 Shimohozumi, Ibaraki, Osaka 567-8680, Japan, [b]Japan Synchrotron Radiation Research Institute, Koto, Sayo, Hyogo 679-5198, Japan, and [c]Department of Materials Science, Nagoya Institute of Technology, Gokiso-cho, Showa-ku, Nagoya 466-8555, Japan. *Correspondence e-mail: tsukasa_miyazaki@gg.nitto.co.jp

Received 22 December 2014
Accepted 22 April 2015

Edited by V. T. Forsyth, Institut Laue-Langevin, France, and Keele University, UK

Keywords: small-angle X-ray scattering; wide-angle X-ray diffraction; stress–strain relationships; three-dimensional structural evaluation.

A simple three-dimensional structural evaluation system for a film during uniaxial deformation has been developed. The system is realized with an automatic film stretching machine, which allows the horizontally symmetric stretching of a film, and a synchrotron radiation X-ray scattering apparatus. Using this system, two-dimensional patterns of small-angle X-ray scattering and wide-angle X-ray diffraction can be obtained simultaneously during film stretching in the so-called edge and end views, together with stress–strain data. As cylindrical symmetry of the structure can be expected for a uniaxially stretched film, the two-dimensional patterns in the through view are identical to those in the edge view, indicating that three-dimensional structural characterization can be performed with a combination of edge and end views during film stretching. For amorphous poly(ethylene terephthalate) and crystalline poly(vinyl alcohol) films, the preliminary results of three-dimensional structural characterization during film stretching are shown.

1. Introduction

It is very important to clarify the relationship between the structure and properties of polymer films for the production of new functional polymer films with various superior properties, such as mechanical toughness and strength. In particular, *in situ* observation of structure in films during processing is crucial for designing functions originating from the structural hierarchy in polymers ranging from sub-nanometre to micrometre length scales, because the films obtain their functions with their structural changes under processing (Ward *et al.*, 2000). To investigate structure in commercially available polymer films during uniaxial deformation, *in situ* structural characterization techniques have recently been developed by combining synchrotron radiation X-ray scattering techniques and an automated film stretching apparatus (Chu & Hsiao, 2001; van Aerle & Braam, 1988; Mahendrasingam *et al.*, 1992, 1995; Hughes *et al.*, 1997, Butler *et al.*, 1995). Small-angle X-ray scattering (SAXS) and/or wide-angle X-ray diffraction (WAXD) measurements with two-dimensional area detectors and simultaneous stress–strain measurements have been performed using these systems.

However, only limited information can be obtained with the general systems reported previously, because they cannot evaluate the three-dimensional structural changes that occur during uniaxial deformation. In general, only two-dimensional scattering patterns in the so-called through view are obtained during uniaxial deformation, by introducing the incident X-rays into the film from the direction normal to the film

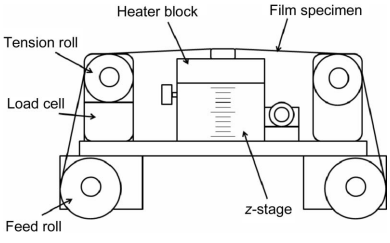

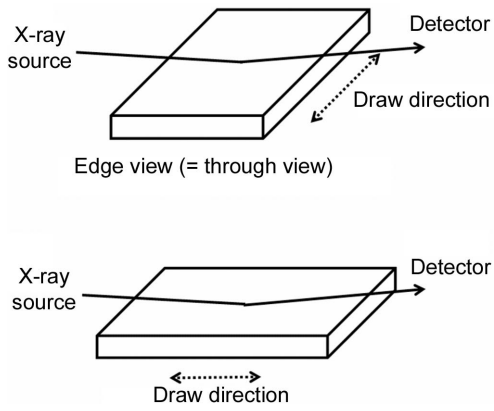

Figure 1
Experimental setups for obtaining edge and end views. The edge view should be identical to the through view when the film is stretched uniaxially.

surface. In the case of the structures within a film during uniaxial deformation, those with cylindrical symmetry around the stretching direction can be expected to evolve in the film. Therefore, the two views from both directions perpendicular to the stretching direction, both the through view and the edge view which is obtained by introducing X-rays from the side of the film, are identical, while the view from the stretching direction (the end view) is quite different, as shown schematically in Fig. 1. Hence, a complete three-dimensional structural evaluation can be performed using a combination of end and edge views of the sample during uniaxial deformation. To obtain two-dimensional scattering patterns in the end view, the incident X-rays are also required to hit the side of the film in the direction parallel to the stretching direction. However, only two-dimensional scattering patterns in the through view have been obtained in the systems constructed previously, as mentioned above. Therefore, the complete three-dimensional structural hierarchy within a film has not been evaluated because of the loss of structural information in the end view.

In this article, we propose a simple three-dimensional structural characterization system combined with a film stretching apparatus and X-ray scattering techniques at a synchrotron radiation facility.

2. System configuration

2.1. General description of the newly developed stretching machine

The film stretching machine, shown schematically in Fig. 2, was designed to stretch both sides of a film horizontally using two feed rolls. The two sides of the film specimen are clamped to the two feed rolls. The central portion of the film is positioned on a heating stage. The two feed rolls are then rotated in opposite directions by a stepping motor, both turning at the same speed through gears, resulting in a symmetric stretching of the film. Therefore, the portion of the film attached to the heating stage does not move during film stretching. One of the two tension rolls has a load cell, allowing it to detect the load applied to the film during the stretching process. The film extension is acquired from the number of pulses sent to the stepping motor. The heating stage is capable of heating the portion of film attached to it up to 523 K. The stretching speed can be changed within the range 0.5–35 mm min^{-1}. The maximum load to which the film is subjected is 200 N during film stretching.

In Fig. 2, when the incident X-rays penetrate the side of the film from the direction normal to the paper, the two-dimensional scattering profile in the edge view can be obtained, identical to that in the through view usually obtained in the case of uniaxial stretching, in which the incident X-rays are introduced into a film from the direction normal to the film surface. On the other hand, when the incident X-ray beam horizontally irradiates the side of the film from the left or right side, the two-dimensional scattering pattern in the end view can be obtained, as shown schematically in Fig. 1. Therefore, rotation of the stretching machine by 90° with respect to the incident direction of the X-rays allows one to obtain *in situ* the two-dimensional X-ray scattering patterns in both edge and end views during film stretching, as shown in Figs. 3(*a*) and 3(*b*). This indicates that *in situ* three-dimensional structural characterization can be performed with a combination of edge and end views, because the remaining through view is identical to the edge view in the case of uniaxial deformation, as mentioned above. The size of the top portion of the heating stage is limited to 12 × 12 mm to prevent line broadening of the diffraction peaks. This is because a wide radiation area of the specimen causes an increase in sample size, especially for grazing-incidence WAXD within several degrees of the grazing-incidence angle, including horizontal radiation, resulting in line broadening of the diffraction peaks (Breiby *et al.*, 2008).

Only the portion of film attached to the heating stage is drawn in the film stretching process, because the other portions of the film are not heated. Therefore, the minimum and maximum stretching speeds mentioned above correspond to stretching rates of 4 and 292% min^{-1}, respectively, on the basis of the initial drawable film length. Moreover, the film on the heating stage must be positioned above the rollers or other portions of the stretching machine by raising the heating stage,

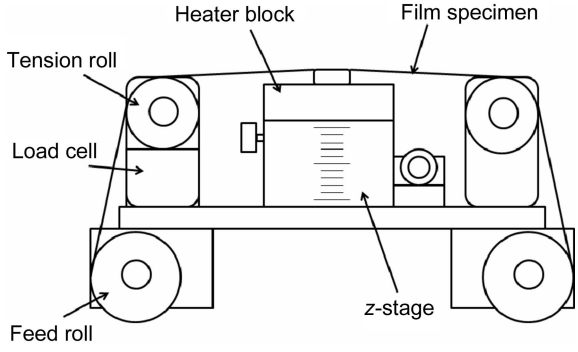

Figure 2
A schematic drawing of the newly developed stretching machine for three-dimensional structural evaluation of polymer films during uniaxial deformation.

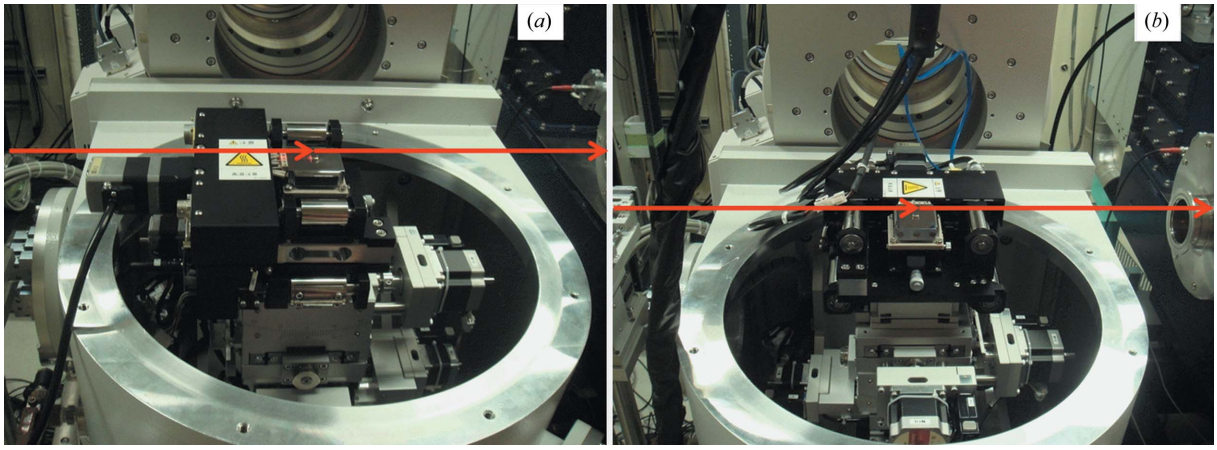

Figure 3
Photographs of both setups for obtaining two-dimensional scattering patterns in (*a*) the edge view and (*b*) the end view. The red arrows in each case indicate the direction of the X-ray beam.

using the height stage on which it is mounted, to enable horizontal irradiation by the incident X-ray beam, as shown schematically in Fig. 2. As a result, three-dimensional structural evaluations can be performed during film stretching with a combination of edge and end views.

2.2. *In situ* true stress–strain measurements

A CCD camera is mounted on the stretching machine to monitor the film width during film stretching. As mentioned above, only the portion of the film attached to the heating stage is heated during film stretching, resulting in stretching of the local portion only. Therefore, the local strain of the stretched portion on the heating stage should not be identical to the macroscopic film strain. The local stress and local strain of the stretched portion of the film horizontally irradiated by the incident X-ray beam can be calculated from the load and film width measured during film stretching, if $W_i/W_0 = D_i/D_0$, where W_i is the real-time film width measured *in situ* by the CCD camera and D_i is the real-time film thickness. The subscript 0 refers to the initial conditions prior to film stretching. The local true strain of the examined portion of the film can be calculated as

$$\frac{L_i - L_0}{L_0} = \left(\frac{W_0}{W_i}\right)^2 - 1, \tag{1}$$

where L_i is the real-time local film length, assuming that the local film volume is kept constant during film stretching, $L_i W_i D_i = L_0 W_0 D_0$.

On the other hand, the local true stress, σ_i, is calculated using the real-time load, F_i, as follows:

$$\sigma_i = \frac{F_i}{W_i D_i} = \frac{F_i W_0}{W_i^2 D_0}. \tag{2}$$

Therefore, the relationship between the local stress and local strain can be evaluated in real time from the film width and the load measured during film stretching (Valladares *et al.*, 2005).

2.3. Simultaneous SAXS/WAXD measurements

Simultaneous SAXS/WAXD measurements were performed on the BL03XU beamline at SPring-8 (Sayo, Hyogo, Japan). Figs. 3(*a*) and 3(*b*) show the setups of this stretching machine in the first hutch of BL03XU for the acquisition of two-dimensional scattering patterns from the edge and end views, respectively. The first hutch was specially designed for grazing-incidence X-ray scattering measurements at this beamline. The basic configurations of BL03XU and the first hutch have been described elsewhere [Masunaga *et al.* (2011) and Ogawa *et al.* (2013), respectively]. The film stretching machine is located on the height stage of the diffractometer in the first hutch. The precise diffractometer system allows the film attached on the heating stage to be aligned so that the incident X-rays accurately hit the side of the film for the edge view (Fig. 3*a*). As shown in Fig. 3(*b*), the end view can be obtained with an automatic 90° rotation of the height stage on which the film stretching machine is mounted.

For the preliminary SAXS/WAXD experiments described in this paper, the X-ray wavelength was tuned to 0.1 nm and the beam size at the sample position was 200 × 100 µm (horizontal × vertical). The sample-to-detector distances were 2325.8 and 153.8 mm for SAXS and WAXD, respectively. The two-dimensional scattering patterns for SAXS and WAXD were collected on a cooled CCD (II+ CCD; Hamamatsu Photonics, V7739P + ORCA-R2) of 1344 × 1024 pixels with a size of 63 µm^2 per pixel with an X-ray image intensifier, and with a flat-panel detector (Hamamatsu Photonics, C9827DK-10) of 1024 × 1024 pixels with a size of 50 µm^2 per pixel, respectively. Basically, the incident X-ray beam irradiates the side of the film at an angle of incidence of 0° (in the direction parallel to the film surface) or within 0.2°. An accurate absorption correction should be performed, because the penetration path lengths of X-rays in the film differ greatly with the scattering angle between the incident X-ray beam and the outgoing one, especially for WAXD data. However, an absorption correction may not be required for polymer films because of their small absorption coefficients (Baker *et al.*, 2010). In this article, an accurate absorption correction is

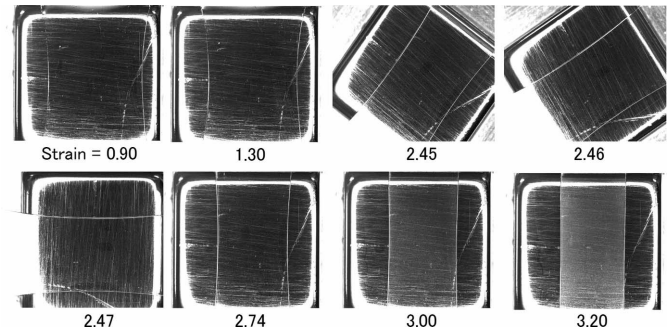

Figure 4
Selected photographs obtained with a CCD camera mounted directly above the heated portion of a sample for real-time measurement of the film width during film stretching at 343 K for the PET film, with strains as indicated.

ignored for the analysis of the preliminary results described in the next section. The precise absorption correction method for WAXD data will be discussed in a future paper. For SAXS data we have already described the absorption correction method (Shimokita *et al.*, 2014).

3. Preliminary results

Typical examples are described in the cases of amorphous poly(ethylene terephthalate) (PET) and crystalline poly(vinyl alcohol) (PVA) films. The PET films were purchased from Teijin Corporation (Japan). The film thickness was 200 µm. The grazing angle of the incident X-rays was 0.2°. The stretching temperatures were 343 and 363 K, and the extension speed was 3 mm min^{-1}. Fig. 4 shows selected photographs taken with a CCD camera mounted directly above the heated portion of the film during film stretching at 343 K. The film width can be estimated accurately from these photographs and used to determine the local true stress and strain, as described in the previous section. The incident X-ray beam irradiates the side of the film horizontally from the left-hand side. Therefore, two-dimensional scattering patterns in the edge view can be obtained for strains of 0.90, 1.30, 2.74, 3.00 and 3.20, whereas those in the end view can be acquired for a strain of 2.47. The final photograph, with a strain of 3.20, indicates that the strain-induced whitening occurs prior to the film breaking and may be due to micro-cracking or micro-crazing.

The macroscopic nominal load–extension relationships at 343 and 363 K are shown in Figs. 5(*a*) and 5(*b*), respectively. They can be converted into the local true stress–strain relationships (Figs. 5*c* and 5*d*) by monitoring the real-time film width and macroscopic load, as described above. We cannot infer the structural transitions within the film based on the nominal load–extension relationships, whereas the local true stress–strain relationships clearly describe the structural changes with strain. That is to say, the true stress–strain relationships cover the three regions with strain, as shown in the general case of film stretching at relatively low temperatures. In Fig. 5(*c*), these three regions are indicated with vertical dotted lines. The film expands elastically with strain in the first

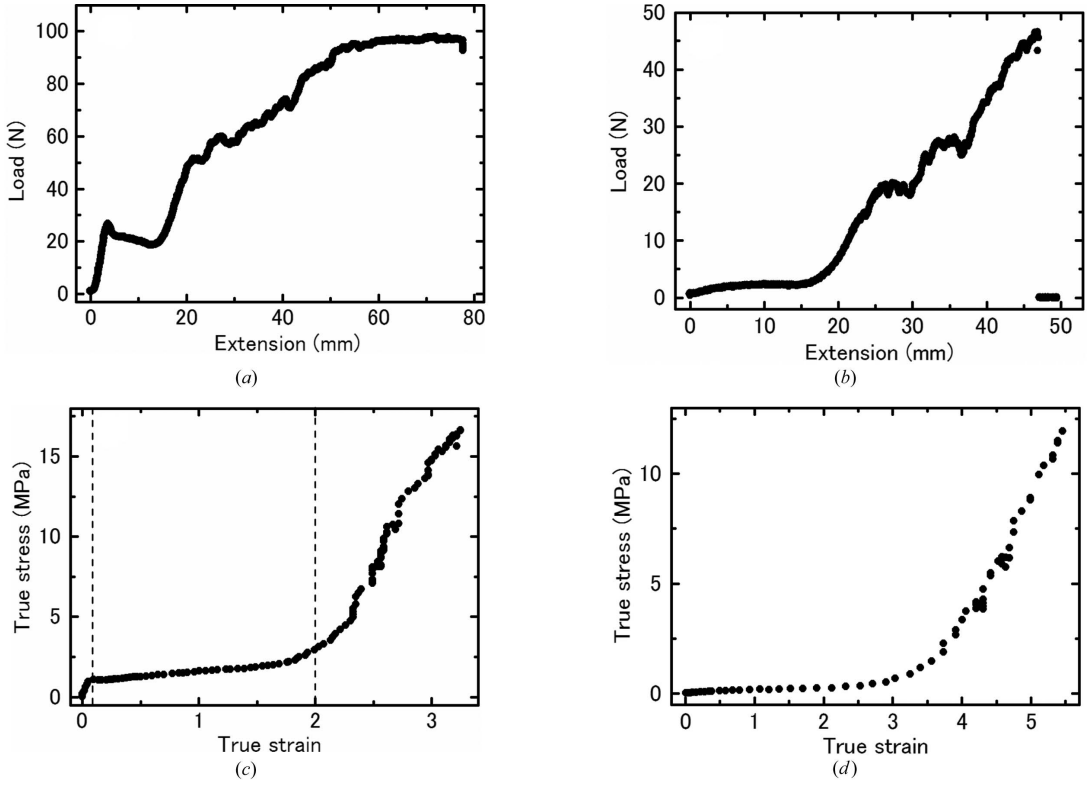

Figure 5
(Top) Nominal macroscopic load–extension relationships for the PET film during stretching at (*a*) 343 K and (*b*) 363 K. (Bottom) Local true stress–strain relationships for the PET film during stretching at (*a*) 343 K and (*d*) 363 K, converted from parts (*a*) and (*b*).

region below a strain of 0.1. In the second region above a strain of 0.1, the stress barely increases with strain. In the third region above a strain of 2.00, strain-induced hardening occurs up to the film breaking. At higher temperatures it is difficult to detect the first region with chain relaxation (Fig. 5*d*).

In situ structural characterization can be performed on the basis of the WAXD patterns obtained during film stretching. The exposure time is 1 s for WAXD, and it takes 10 s to exchange the experimental geometry from that for obtaining an edge view to that for obtaining an end view. Fig. 6 shows the stress–strain relationship and selected two-dimensional WAXD patterns in the edge and end views obtained during film stretching at 343 K. The scattering pattern in the edge view is identical to that in the end view for the film with a strain of 0, indicating that the film has a homogeneous structure prior to stretching. The scattering pattern in the edge view can change with film stretching, as shown in the through view obtained by a generally available stretching machine for *in situ* observations. On the other hand, the scattering pattern in the end view is almost unchanged during film stretching.

The edge view two-dimensional WAXD patterns were analysed to estimate the crystallinity index in the film during film stretching, as described in the usually available film stretching experiments in which only the through views are examined upon film drawing. One-dimensional diffraction profiles were obtained with azimuthal integration within a range of 90° from the out-of-plane direction to the in-plane direction in the two-dimensional WAXD patterns (Miyazaki *et al.*, 2010). A typical example of the azimuthally integrated diffraction profile is shown in Fig. 7 for the film with a strain of 2.00 during film stretching at 343 K. To determine the apparent crystallinity index in the film, a peak decomposition procedure was performed on these one-dimensional profiles obtained during uniaxial deformation. The one-dimensional scattering profiles were decomposed into three crystalline peaks, 010, $\bar{1}10$ and 100, and one amorphous halo in the examined 2θ region. The peak type was chosen to be Gaussian.

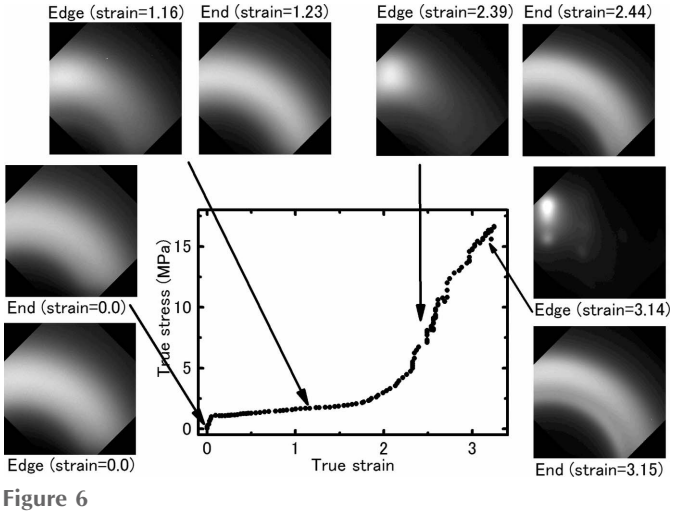

Figure 6
Local true stress–strain relationships and selected two-dimensional WAXD patterns, with strains as indicated by arrows, during film stretching at 343 K for the PET film.

In the peak fitting procedure, the only fixed parameter is the full width at half-maximum (FWHM) of the amorphous peak, which can be evaluated from the azimuthally integrated diffraction profile of an undrawn sample. Other parameters (positions, heights and FWHMs of the three crystalline peaks, and the position and height of the amorphous peak) were allowed to float in the fitting routine. A typical fitting result for the film with a strain of 2.00 is also shown in Fig. 7. The apparent crystallinity index, f_c, is thus determined as

$$f_c = \frac{\sum A_c}{\sum A_c + A_a}, \tag{3}$$

where A_c is the integrated area underneath the crystalline peaks and A_a is the integrated area of the amorphous peak. These analytical methods have frequently been used to estimate crystallinity for two-dimensional WAXD patterns in the through view during uniaxial deformation of polymers (Wu *et al.*, 2003; Nogales *et al.*, 2003; Miyazaki *et al.*, 2007).

The crystallinity indices during film stretching at 343 and 363 K are summarized in Figs. 8(*a*) and 8(*b*), respectively, with the corresponding local stress–strain relationships. The analytical method mentioned above can only be applied to data which include the crystalline diffraction peaks. The crystalline peaks are detectable in the data at strains above about 2.0 and 3.5 (the third regions) for the film stretching experiments at 343 and 363 K, respectively, as shown in Figs. 8(*a*) and 8(*b*). In the third regions it can be clarified that strain-induced crystallization occurs accompanied by strain-induced hardening. In Fig. 6, this is clearly confirmed by the oriented crystalline diffraction in the two-dimensional scattering patterns in the edge view at strains above 2.00. Even in the two-dimensional patterns in the end view, the crystalline diffraction appears on the lower side of the amorphous halo above a strain of 2.00, as shown in Fig. 6. This increase in the crystallinity index accompanies the stress increase, clearly indicating that the stress increase should be attributed to hardening with crystallization in the film. On the other hand, in the first and second regions, a mesomorphologic phase or an oriented amorphous phase must be produced with film

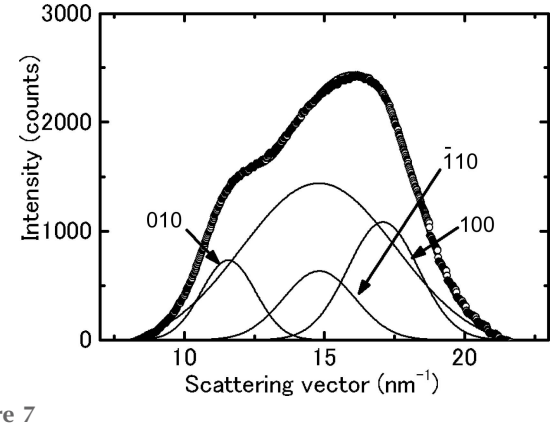

Figure 7
A typical example of the peak decomposition of an azimuthally integrated diffraction profile for a two-dimensional WAXD pattern in the edge view with a strain of 2.00 on film stretching for the PET film. Points are experimental data and lines are the best fitting curves.

stretching, shown schematically in the edge view at a strain of 1.16 in Fig. 6 (Kawakami *et al.*, 2003, 2004).

The case of the PVA film during stretching at 403 K is shown in Fig. 9. For the undrawn sample, the SAXS and WAXD scattering patterns in the end view are identical to those in the edge view, implying that the structure, over length scales ranging from sub-nanometre to several tens of nanometres, is homogeneous prior to film stretching, as also shown for PET stretching. On stretching the PVA film, the two-dimensional WAXD pattern in the end view is almost unchanged, while that in the edge view describes oriented structures in the film. As shown in Fig. 10, the orientation function of these crystallites increases with increasing strain, which is evaluated using the azimuthal plots of the 110 and $1\bar{1}0$ doublet crystalline diffraction peaks in the two-dimensional WAXD patterns (Miyazaki *et al.*, 2007, 2010). The SAXS pattern also changes drastically during film stretching, for both end and edge views. On the lamellar scale, uniaxially oriented structures corresponding to the crystalline orientation function described in Fig. 10 are also expected to appear in edge-view two-dimensional SAXS patterns with strain. This is shown by the pair of vertical streaks in the edge view SAXS pattern at a strain of 3.69 in Fig. 9.

In contrast, the SAXS intensity originating from the lamellar structures is reduced in the end view two-dimensional SAXS patterns during film stretching, owing to lamellar orientation in the direction parallel to the stretching direction. However, circular diffuse scattering also appears in the two-dimensional SAXS patterns at a different scattering angle from the scattering peak position originating from the long period with strain, and this is illustrated in the end view two-dimensional SAXS pattern with a strain of 1.00. This diffuse scattering in the two-dimensional SAXS pattern may correspond to streak scattering with a peak in the two-dimensional pattern in the through view for a dried specimen after drawing in water (Miyazaki *et al.*, 2005). Streak scattering in uniaxially deformed films can originate from various scatterers, such as nano-cracking, nano-voids and microfibrils. In the case of PVA films stretched in water, this streak scattering might be attributed to microfibrillation (Miyazaki *et al.*, 2006, 2007.). Therefore, this diffuse scattering may originate from the correlation length between microfibrils in the case of two-dimensional scattering patterns in the end view, although the PVA film reported in this article is uniaxially deformed in air. We will publish a detailed structural characterization of the

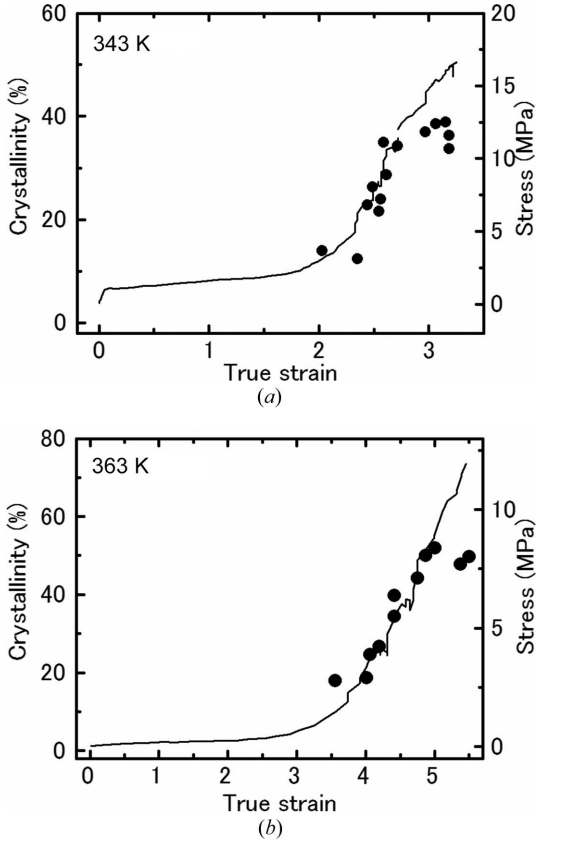

Figure 8
Crystallinity indices and the local true stress–strain relationships during film stretching at (*a*) 343 K and (*b*) 363 K for the PET film.

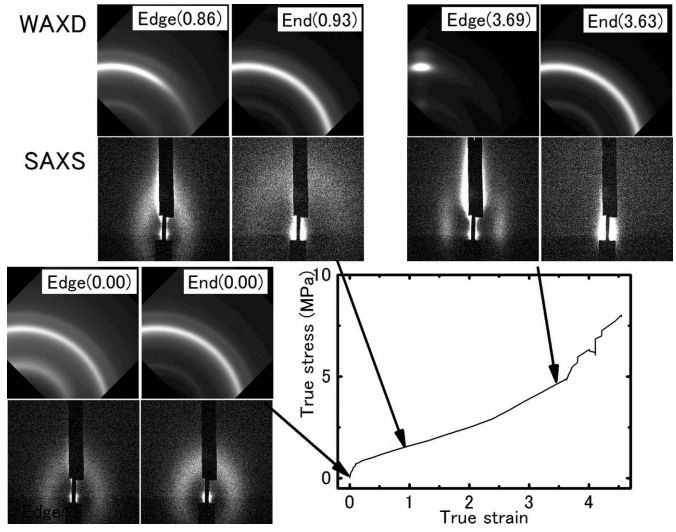

Figure 9
Local true stress–strain relationships and selected two-dimensional SAXS and WAXD patterns, with strains as indicated by arrows and numerical values in parentheses, during film stretching at 403 K for the PVA film.

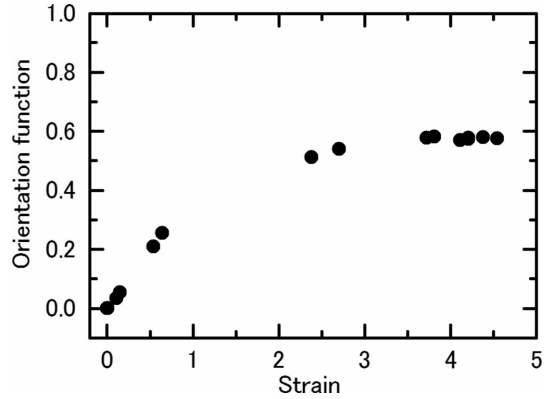

Figure 10
Orientation function deduced from the azimuthal plots of the 110 and $1\bar{1}0$ doublet crystalline diffraction peaks.

PVA film elsewhere, combined with information obtained exclusively from the end view. These *in situ* three-dimensional structural evaluations are valid for investigating the relationship between structure and properties in polymers under processing, because the three-dimensional structures within polymers may change drastically under different conditions.

In conclusion, we have developed a new film stretching machine combined with a synchrotron SAXS/WAXD apparatus, allowing us to evaluate *in situ* the three-dimensional structural evolution within polymer films during film stretching. It has been successfully demonstrated that the three-dimensional structural changes within an amorphous PET film and a crystalline PVA film can be evaluated during uniaxial deformation.

Acknowledgements

The synchrotron radiation experiments were performed on beamline BL03XU at SPring-8 with the approval of the Japan Synchrotron Radiation Research Institute (Proposal Nos. 2013A7216 and 2013B7264).

References

Aerle, N. A. J. M. van & Braam, A. W. M. (1988). *J. Appl. Cryst.* **21**, 106–108.
Baker, J. L., Jimison, L. H., Mannsfeld, S., Volkman, S., Yin, S., Subramanian, V., Salleo, A., Alivisatos, A. P. & Toney, M. F. (2010). *Langmuir*, **26**, 9146–9151.
Breiby, D. W., Bunk, O., Andreasen, J. W., Lemke, H. T. & Nielsen, M. M. (2008). *J. Appl. Cryst.* **41**, 262–271.
Butler, M. F., Donald, A. M., Bras, W., Mant, G. R., Derbyshire, G. E. & Ryan, A. J. (1995). *Macromolecules*, **28**, 6383–6393.
Chu, B. & Hsiao, B. (2001). *Chem. Rev.* **101**, 1727–1762.
Hughes, D. J., Mahendrasingam, A., Oatway, W. B., Heeley, E. L., Martin, C. & Fuller, W. (1997). *Polymer*, **38**, 6427–6430
Kawakami, D., Hsiao, B. S., Ran, S., Burger, C., Fu, B., Sics, I., Chu, B. & Kikutani, T. (2004). *Polymer*, **45**, 905–918.
Kawakami, D., Ran, S., Burger, C., Fu, B., Sics, I., Chu, B. & Hsiao, B. S. (2003). *Macromolecules*, **36**, 9275–9280.
Mahendrasingam, A., Fuller, W., Forsyth, V. T., Oldman, R. J., MacKerron, D. & Blundell, D. J. (1992). *Rev. Sci. Instrum.* **83**, 1087–1090.
Mahendrasingam, A., Martin, C., Jaber, A., Hughes, D., Fuller, W., Rule, R., Oldman, R. J., MacKerron, D. & Blundell, D. J. (1995). *Nucl. Instrum. Methods Phys. Res. Sect. B*, **97**, 238–241.
Masunaga, H. *et al.* (2011). *Polym. J.* **43**, 471–477.
Miyazaki, T., Hoshiko, A., Akasaka, M., Sakai, M., Takeda, Y. & Sakurai, S. (2007). *Macromolecules*, **40**, 8277–8284.
Miyazaki, T., Hoshiko, A., Akasaka, M., Shintani, T. & Sakurai, S. (2006). *Macromolecules*, **39**, 2921–2929.
Miyazaki, T., Katayama, S., Funai, E., Tsuji, Y. & Sakurai, S. (2005). *Polymer*, **46**, 7436–7442.
Miyazaki, T., Takeda, Y., Akane, S., Itou, T., Hoshiko, A. & En, K. (2010). *Polymer*, **51**, 5539–5549.
Nogales, A., Sics, I., Ezquerra, T. A., Denchev, Z., Balta Calleja, F. J. & Hsiao, B. S. (2003). *Macromolecules*, **36**, 4827–4832.
Ogawa, H. *et al.* (2013). *Polym. J.* **45**, 109–116.
Shimokita, K., Miyazaki, T., Ogawa, H. & Yamamoto, K. (2014). *J. Appl. Cryst.* **47**, 476–481.
Valladares, B., Yalcin, B. & Cakmak, M. (2005). *Macromolecules*, **38**, 9229–9242.
Ward, I. M., Coates, P. D. & Dumoulin, M. M. (2000). *Solid Phase Processing of Polymers.* Munich: Hanser Publishers.
Wu, J., Schultz, J. M., Yeh, F., Hsiao, B. S. & Chu, B. (2003). *Macromolecules*, **33**, 1765–1777.